This article has been accepted for publication in IEEE Transactions on Automation Science and Engineering. This is the author's version which has not been fully edited and content may change prior to final publication. Citation information: DOI 10.1109/TASE.2026.3748659

High-speed tracking control of dielectric elastomer actuators with coupled nonlinearities via modified robust repetitive control strategy

Peinan Yan, Sumeet S. Aphale, Jiang Zou, and Guoying Gu

***Abstract*—High-speed dielectric elastomer actuators (HDEAs), featuring large strain and high frequency-response, provide a new avenue for robotic systems. However, their dynamic responses suffer from rate-dependent viscoelasticity, mechanical vibration, temperature drift, and their couplings, posing significant challenges for high-precision control. To address this issue, this work proposes a modified robust repetitive control (MRRC) strategy for HDEAs to mitigate such intricate nonlinearities. Firstly, we conduct systematic experiments on the nonlinear dynamics in one HDEA (natural frequencies of 120 and 230 Hz). For dynamic model simplification, the rate-dependent viscoelasticity and creep-and-heating-induced displacement drift are treated as a periodic and sustaining disturbance, respectively. Thus, a cascading dynamic model incorporating an electromechanical transduction unit is established to characterize the dynamic response. Next, the MRRC is developed by establishing a stable approximate inverse model and integrating a band-stop filter. Finally, various tracking results demonstrate that our MRRC can effectively compensate for rate-dependent viscoelasticity, mechanical vibrations, and temperature drift across a wide frequency range. The maximum working frequency reaches 270 Hz, while the maximum tracking error is less than 3.49%. Moreover, the HDEA achieves a resolution of 75 nm with a stroke of 144 μm, paving the way for DEA-based micro-manipulation systems.**

***Note to Practitioners*—The motivation of this work is to mitigate the coupled rate-dependent viscoelasticity, mechanical vibration, and temperature drift in the high-speed dielectric elastomer actuators (HDEAs), thus achieving high-precision tracking control. Though HDEAs have been widely applied in soft robots and wearable systems, their nonlinear dynamic compensation remains challenging due to the complex nonlinearity. The rate-dependent viscoelasticity across a wide frequency spectrum raises great challenges in nonlinearity compensation. The mechanical vibration and accompanying frequency- and time-related temperature drift are further coupled with the rate-dependent viscoelasticity, generating a pressing need for an effective control method. This work presents a modified robust repetitive control strategy to address this issue. Based on a systematic study of dynamic response and proper simplification, a series dynamic model is established. Its inverse model enables the introduction of the repetitive control (RC) strategy. Then, integrating a band-stop filter in the control scheme suppresses the gain amplification at non-harmonics. The proposed MRRC scheme achieves high-precision and high-speed control of the HDEA, which can be implemented in dielectric-actuated high-precision manipulation systems in medical scenarios.**

***Index Terms*—Dielectric elastomer actuators, rate-dependent viscoelasticity, mechanical resonance, temperature drift, modified robust repetitive control, soft robots.**

I. Introduction

DIELECTRIC elastomer actuators (DEAs), known as a family of electric-driven artificial muscles, demonstrate large strain [1], high energy density [2], and lightweight nature [3]. Generally, a DEA comprises a dielectric elastomer membrane sandwiched by compliant electrodes [4]. With an external voltage, the Coulomb force between the opposite charges compresses the intermediate elastomer, causing its thickness decrease and simultaneous area expansion [5]. Based on the actuation principle, various actuator configurations have been designed to generate different deformations, including rolled [6], stacked [7], and planar DEAs [8]. Recently, by employing silicone and carbon nanotubes as dielectric elastomer and compliant electrodes, respectively, high-speed DEAs (HDEAs) have been designed [9], demonstrating increased bandwidth (over 200 Hz) and high power density. The developed actuators further spawn robotic systems, including wearable systems [10], crawling robots [11], and aerial robots [12]. Their extensive applications generate urgent requirements for high-precision tracking control [11].

However, the dynamic response of the HDEA suffers from intricate nonlinearities: i) the rate-dependent viscoelasticity. As a viscoelastic material, the HDEA demonstrates both creep and hysteresis effects [13]. Specifically, the creep effect causes the slow-time displacement drift in the initial operating time. The hysteresis is an asymmetric, multivalued, and rate-dependent nonlinearity throughout the actuation; ii) mechanical vibration. The resonance phenomena lead to mechanical vibration in certain frequency ranges [14]; iii) temperature drift. Originating from the electrode resistance and the viscoelastic damping of the elastomer, the dissipation of input electrical energy during charging and discharging finally induces sustained heat generation, which becomes prominent in high-frequency operation [12]. This manifests as a frequency- and time-related disturbance in the output displacement, thereby further deteriorating the actuating accuracy [15]. The intertwining of the above nonlinearities provides significant difficulties in high-precision control of HDEAs.

To compensate for the intricate nonlinearity of DEAs, various control strategies have been developed over the past two decades, which can be categorized into four kinds, including physics-based, phenomenological, lumped-parameter-

Peinan Yan, Jiang Zou, and Guoying Gu are with the State Key Laboratory of Mechanical System and Vibration, School of Mechanical Engineering, Shanghai Jiao Tong University, Shanghai 200240, China, and also with the Shanghai Key Laboratory of Intelligent Robotics, Shanghai Jiao Tong University, Shanghai 200240, China. Sumeet S. Aphale is with the Artificial Intelligence, Robotics and Mechatronic Systems Group (ARMS), School of Engineering, University of Aberdeen, UK. (Corresponding authors: Jiang Zou; Guoying Gu. E-mail: peinanyan@sjtu.edu.cn; s.aphale@abdn.ac.uk; zoujiang@sjtu.edu.cn; guguoying@sjtu.edu.cn)

This work was supported by the National Key R&D Program of China (Grant no. 2024YFB4707500), the Shanghai Eastern Talent Plan (Youth Project) (Grant No. QNKJ2025060), the Young Elite Scientists Sponsorship Program by CAST (Grant No. YESS20240487), and the State Key Laboratory of Mechanical System and Vibration (Grant No. MSVZD202605).

Authorized licensed use limited to: Shanghai Jiaotong University. Downloaded on November 05,2026 at 09:43:44 UTC from IEEE Xplore. Restrictions apply.
© 2026 IEEE. All rights reserved, including rights for text and data mining and training of artificial intelligence and similar technologies. Personal use is permitted, but republication/redistribution requires IEEE permission. See https://www.ieee.org/publications/rights/index.html for more information.

This article has been accepted for publication in IEEE Transactions on Automation Science and Engineering. This is the author's version which has not been fully edited and content may change prior to final publication. Citation information: DOI 10.1109/TASE.2026.3748659

based, and learning-based controllers. Modeling the dielectric elastomer as a hyperelastic material (i.e., Neo-Hookean model [16]) enables a precise description of the electromechanical deformation [17]. Meanwhile, the inherent viscoelasticity is regarded as an energy-dissipative phenomenon [18]. Incorporating rheological units into the constitutive model facilitates dynamic response description [19], which further motivates advanced controller design (i.e., nonlinear PID [20]). However, the contained differential equations impose considerable difficulties on the controller conversion. To overcome this drawback, phenomenological controllers have been developed [21]. Their applications primarily rely on quantitative characterization of the hysteresis effect through phenomenological models (i.e., Duhem model [22], Prandtl-Ishlinskii model [23]). Through their direct or implicit inverse [23], [24], the rate-dependent viscoelasticity can be effectively compensated. Also, the identified model provides fundamental supports in developing fuzzy controllers [25]. However, the phenomenological models neglect the intrinsic mechanical structure, making them incapable of capturing mechanical vibration. Consequently, the corresponding controllers are restricted to low-frequency operation. To address this limitation, the DEA is further simplified as a lumped-parameter system [26]. This operation enables describing the coupled rate-dependent viscoelasticity and mechanical vibration over a wide frequency range, hence greatly facilitating related controller design (i.e., robust control [27], sliding-mode control [28]). Recently, machine learning has demonstrated significant potential in nonlinearity compensation [29]. Through the dataset establishment and training process, the developed learning-based controllers have achieved high-precision trajectory tracking in both open- and closed-loop cases [30], [31]. However, existing controllers are mainly verified in a low working frequency range. For the HDEAs, the nonlinearity becomes more complicated in a high-speed operation ($>$200 Hz), thus leaving the high-speed tracking of HDEAs a critical issue.

Repetitive control (RC) has been verified to deliver high-precision asymptotic tracking for periodic references [32], [33]. However, the coupled nonlinearity in the HDEA raises great challenges in its application. To address this challenge, this work proposes a modified robust repetitive control (MRRC) scheme to compensate for the complex nonlinearity of HDEAs. Firstly, a customized experimental platform is established to characterize the nonlinear response of a stacked DEA. Dynamic performance tests reveal its high natural frequencies (120 and 230 Hz), rate-dependent viscoelasticity within a wide frequency range, and accompanying temperature drift phenomenon. Based on the dynamic response analysis, the HDEA is first assumed to be a series-parallel system. The model consists of an electromechanical transduction unit, a viscoelasticity module, and a linear system connected in series, along with a heating module in parallel. To introduce the RC strategy, the rate-dependent viscoelasticity and creep-and-heating-induced displacement drift are regarded as a bounded periodic disturbance and a sustaining slow disturbance, respectively. Hence, the model can be simplified into a cascading system including an electromechanical transduction module and a linear system. Its stable approximate model inversion can be obtained via a zero-phase-tracking algorithm. Then, a band-stop filter is designed and integrated into the controller scheme for suppressing the gain amplification at nonharmonic frequencies. The experimental results reveal that the MRRC scheme can achieve high-precision tracking of the HDEA up to 270 Hz. The MRRC strategy mitigates the coupled rate-dependent viscoelasticity, structural vibration, and temperature drift of the HDEA. Various applications solidify its efficacy in achieving high-precision and high-speed control of the HDEA. Further discussion investigates the key factors influencing the tracking performance.

The subsequent sections are organized as follows. Section II begins with the experimental platform design actuated by the HDEA. Moreover, the dynamic tests reveal the intrinsic nonlinearity in this section. Section III presents the detailed establishment of the MRRC scheme. Validation of disturbance decomposition and closed-loop stability is also presented. Then Section IV provides the experimental results through MRRC employment. Section V provides a further discussion, exploring the key controller settings and potential application cases. In the end, Section VI concludes this work and gives a brief outlook for future avenues.

II. Experimental platform

This section commences with the design and fabrication of HDEA. Afterward, a concise overview of the experimental setup is presented. Finally, a comprehensive characterization of the dynamic response in HDEA is conducted in this section.

A. Design and fabrication of HDEA

For proof-of-concept testing, a stacked HDEA is first designed and fabricated [34]. Its fabrication process mainly includes the key steps:

i) Utilizing the Zehntner ZAA 2300 film applicator, the liquid silicone films (Elastosil P7676 and Sylgard 170, mixed ratio of 10:1) are blade cast on a PET film substrate. Then the thin silicone films are cured at 80 $^{\circ}C$ for 10 min.

ii) The compliant electrodes (single-walled carbon nanotubes from XFNANO Inc.) are stamped onto the cured films via a customized mask. Repeating these steps allows creating the multilayer dielectric elastomer with alternatively arranged electrodes. The fabricated one contains 13 layers of dielectric elastomer and 12 layers of compliant electrodes (20 μm for the outer layers and 40 μm for the inner layers).

iii) Stacking the aforementioned multilayer modules enables the creation of the multilayer stacked DEA. Since decreasing the height will improve the operating bandwidth while decreasing the stroke, the stacked DEA is designed with a height of 5 mm to balance the reachable space and response speed. Carbon grease (MG Chemical 846-80G) is then applied for electrical connection.

The high-frequency actuation of the HDEA stimulates the mechanical resonance, causing the unexpected terminal's shaking, thus hindering the high-accuracy measurement [35]. To enhance system stability and enable high-precision measurement under high-frequency actuation, a soft antagonism is symmetrically arranged, which is cast by Elastosil P7676. Its

Authorized licensed use limited to: Shanghai Jiaotong University. Downloaded on November 05,2026 at 09:43:44 UTC from IEEE Xplore. Restrictions apply.
© 2026 IEEE. All rights reserved, including rights for text and data mining and training of artificial intelligence and similar technologies. Personal use is permitted, but republication/redistribution requires IEEE permission. See https://www.ieee.org/publications/rights/index.html for more information.

This article has been accepted for publication in IEEE Transactions on Automation Science and Engineering. This is the author's version which has not been fully edited and content may change prior to final publication. Citation information: DOI 10.1109/TASE.2026.3748659

cross-section and length are the same as those of the used HDEA. The stacked HDEA and the antagonistic structure are respectively connected to the 3D-printed base through one laser-cut acrylic connector. Then they are connected to the opposite face of the terminal using the linear rail, forming an antagonistic structure. The excitation voltage leads to the height decrease and simultaneous area expansion of the stacked DEA. Its electric-induced contraction is then transferred to the translational displacement of the terminal (Fig. 1).

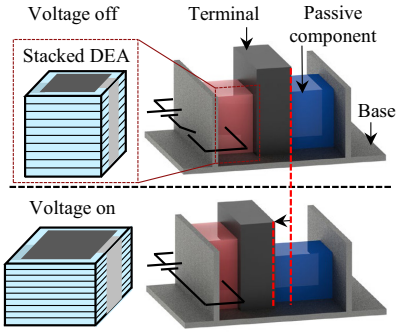


Fig. 1. Design of the HDEA.

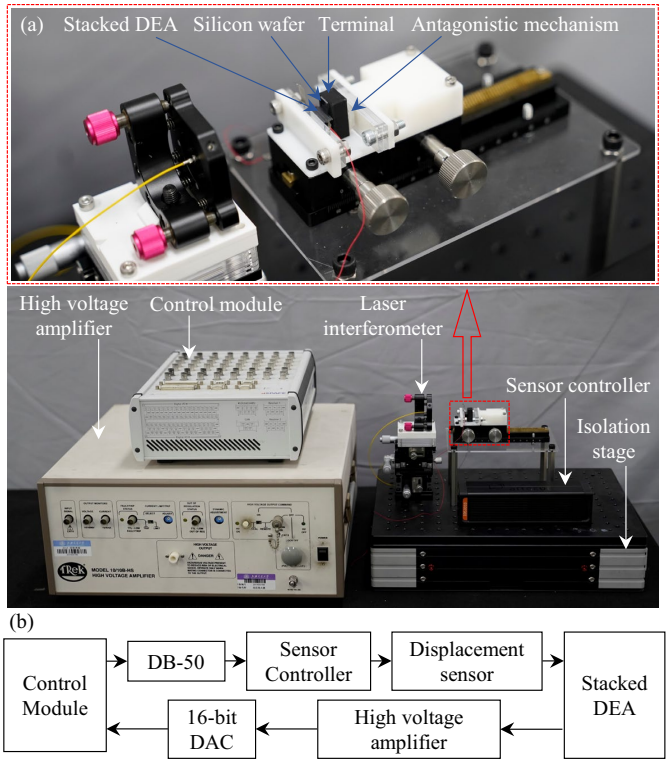


Fig. 2. Experimental setup. (a) Experimental setup and the HDEA prototype. (b) Block diagram representation.

B. Experimental setup

To evaluate its performance and validate the efficacy of our control strategy, a customized experimental setup is established as shown in Fig. 2. The setup mainly consists of the aforementioned HDEA prototype, a laser interferometer (D4/F17, resolution of 25 nm, attocube, Germany), a sensor controller (IDS3010, attocube, Germany), a high-voltage amplifier (Trek 10/10B-HS, fixed gain of 1000, TREK, USA), and a control module (MicroLabBox, dSPACE, Germany). The high-voltage amplifier is employed to provide controllable voltages to the HDEA. The laser interferometer measures the terminal's translational motion, which is then processed by the sensor controller and translated to the control module. Here, a silicon wafer is adhered to the terminal for laser reflection. The control module is responsible for receiving the displacement signal and generating the control signal. The whole platform prototype is placed on an isolation stage (Nano 30, Accurion, Germany). The sampling rate is set to 10 kHz. To avoid performance attenuation in long-term actuation, the voltage saturation is set from 0 to 700V in the following sections.

C. Open-loop characterization

To reveal the frequency response of the HDEA, a sweep frequency test is first conducted. The excitation voltage can be defined as:

$$V_{sweep}(t) = \frac{A}{2}\sin\left[\pi\left(\frac{f_U - f_L}{T}t + f_L\right)t - \frac{\pi}{2}\right] + \frac{A}{2} \quad (1)$$

where A and T represent the amplitude and duration of the input voltage, respectively, while f_U and f_L refer to the upper and lower frequency bounds, respectively. To avoid electrical breakdown, A is set to 700 V, while the other three parameters are flexibly adjusted based on the dynamic responses, satisfying a frequency increase of 4 Hz/s. The experimental results are illustrated in Fig. 3(a), generating key observations:

1) In the low-frequency range, the displacement amplitude first decreases with increasing excitation frequency.

2) As the frequency further increases, the induced structural resonances (120 and 230 Hz) lead to serious mechanical vibration in certain frequency ranges.

3) In the high-frequency range, the reachable displacement range quickly decreases with increasing frequency.

4) In the high-frequency range, persistent displacement drift is noticed, which may be attributed to the heating phenomenon.

To further reveal the rate-dependent viscoelasticity and temperature drift in the actuation, a sinusoidal voltage is applied as:

$$V_{sin}(t) = \frac{A}{2}\sin\left(2\pi f t - \frac{\pi}{2}\right) + \frac{A}{2} \quad (2)$$

where A and f represent the amplitude and frequency of the input voltage, respectively. Key discoveries can be generated:

i) As illustrated in Fig. 3(b), the hysteresis effect manifests different phase delays within the rising and falling stages in one operating period, thus generating an asymmetric hysteresis loop between the input voltage and the output displacement.

ii) Across a wide frequency spectrum, the hysteresis exhibits different forms, indicating a rate-dependent property (Fig. 3b).

iii) To provide a visual demonstration of temperature change, the thermal images are taken under different operating

Authorized licensed use limited to: Shanghai Jiaotong University. Downloaded on November 05,2026 at 09:43:44 UTC from IEEE Xplore. Restrictions apply.
© 2026 IEEE. All rights reserved, including rights for text and data mining and training of artificial intelligence and similar technologies. Personal use is permitted, but republication/redistribution requires IEEE permission. See https://www.ieee.org/publications/rights/index.html for more information.

This article has been accepted for publication in IEEE Transactions on Automation Science and Engineering. This is the author's version which has not been fully edited and content may change prior to final publication. Citation information: DOI 10.1109/TASE.2026.3748659

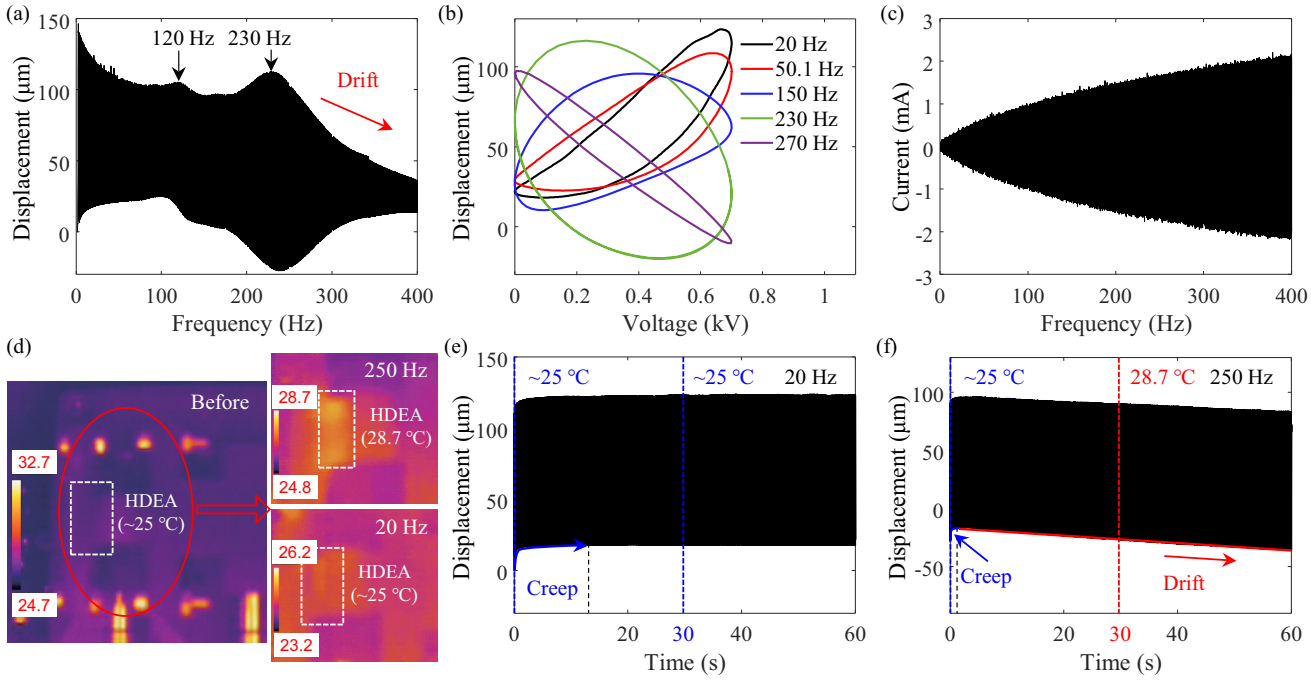


Fig. 3. Dynamic response characterization. (a) Amplitude-frequency characteristic. (b) Hysteresis loops within a wide frequency spectrum. (c) Real-time current in the chirp experiment. (d) Thermal images, taken after being excited for 30 seconds at different frequencies. Responses with sinusoidal voltages of (e) 20 Hz and (f) 250 Hz.

frequencies, as presented in Fig. 3(d). It can be seen that the HDEA becomes hotter after 30 seconds of operation at 250 Hz. However, the 20 Hz input voltage does not cause an obvious temperature change. Correspondingly, the output displacement first drifts in the contraction direction due to the creep effect. Then the accumulated heat in the high-frequency actuation leads to sustained and finite displacement drift in the opposite direction (Fig. 3f), which involves a non-monotonic transition from the creep phenomenon to heating-induced behavior. By comparison, only the creep effect can be observed at the low frequency (Fig. 3e).

It should be mentioned that, except for the part that converts to mechanical energy, the input electrical power is dissipated by the system's damping effect, which derives from the elastomer's viscoelasticity and the system's resistance. Fig. 3(c) demonstrates the input current in the chirp experiment. It can be seen that the input current surges with increasing frequency. As a result, the generated heat is negligible at low operating frequencies. But in the high-frequency range, the HDEA is continually charged and discharged with a high current, leading to heat accumulation and thus temperature drift. Hence, the above phenomena manifest as frequency- and time-related heating, further deteriorating the tracking accuracy.

Overall, the coupling of the mechanical vibration, rate-dependent viscoelasticity, and the aforementioned temperature change leads to significant tracking errors. To achieve high-precision control, the intertwined nonlinearity should be mitigated altogether.

III. Controller Design

The HDEA exhibits high natural frequencies yet complex nonlinearity due to its material properties. The inherent viscoelasticity becomes complicated in the high-frequency range, which is coupled with mechanical vibration over a broad frequency range (>200 Hz). Affected by temperature drift, the high-speed tracking of HDEA still remains a tough problem. The repetitive control (RC) strategy has demonstrated remarkable capability in achieving high-precision asymptotic tracking of periodic references with finite robustness. Nevertheless, the coupled nonlinearity in the HDEA raises great difficulty in its implementation. To handle this issue, the rate-dependent viscoelasticity and the creep-and-heating-induced drift are treated as a bounded periodic disturbance and a sustained slow disturbance in the displacement, respectively. This simplification enables the construction of a series system to capture the dynamic responses, which further facilitates the development of the RC strategy. Based on the transfer function analysis, the control scheme structure is configured, enabling closed-loop frequency response regulation by direct filter design. Then a band-stop filter is designed, forming an attenuation band around the effective frequency. On this basis, a modified robust repetitive control scheme (MRRC) tailored for HDEA is established.

A. Controller structure

The repetitive control (RC) strategy is generally based on a linear internal model [36], whereas the inherent nonlinearity of HDEA hinders its implementation. Based on the above dynamic response analysis, a parallel-series dynamic model is first established to describe the dynamic response of the

Authorized licensed use limited to: Shanghai Jiaotong University. Downloaded on November 05,2026 at 09:43:44 UTC from IEEE Xplore. Restrictions apply.
© 2026 IEEE. All rights reserved, including rights for text and data mining and training of artificial intelligence and similar technologies. Personal use is permitted, but republication/redistribution requires IEEE permission. See https://www.ieee.org/publications/rights/index.html for more information.

This article has been accepted for publication in IEEE Transactions on Automation Science and Engineering. This is the author's version which has not been fully edited and content may change prior to final publication. Citation information: DOI 10.1109/TASE.2026.3748659

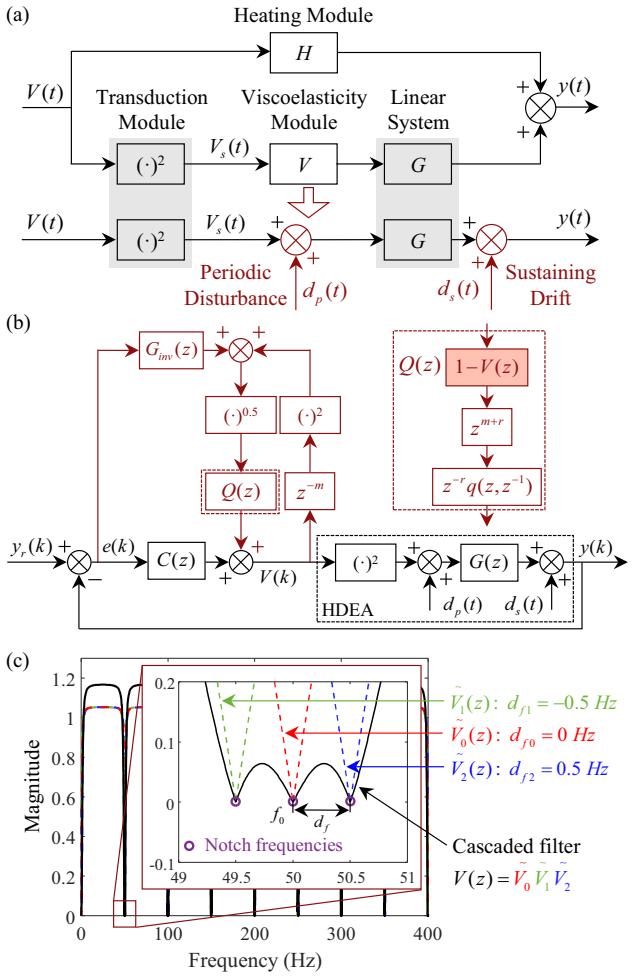


Fig. 4. The MRRC method. (a) Dynamic model of the HDEA. (b) The block diagram of the MRRC scheme. (c) The development of the band-stop filter $V(z)$.

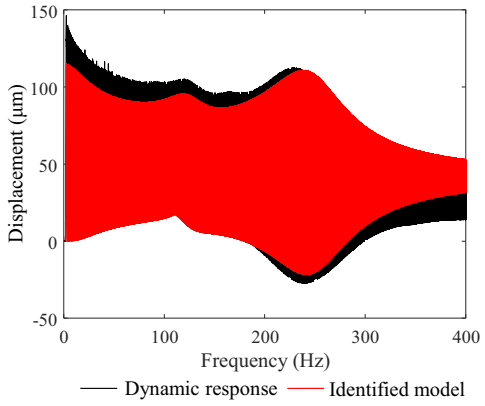


Fig. 5. Validation of the cascading dynamic model.

HDEA. It contains an electromechanical transduction unit, a viscoelasticity module, and a linear system in series, with a heating module arranged in parallel. In the periodic-actuation scenarios, the error arising from viscoelasticity demonstrates periodic and bounded characteristics. So, the rate-dependent viscoelasticity can be treated as a periodic bounded disturbance $d_p(t)$. The temperature drift is a complex phenomenon related to multiple factors (i.e., material, external heat transfer, and so on). It introduces a frequency-related, persistent, and unidirectional displacement drift, which further couples with the creep effect. Given such characteristics, it can be treated as a sustaining slow disturbance $d_s(t)$ in the output displacement.

Remark: Though the creep effect causes displacement drift in the initial phase, it can be mitigated by both feedforward and feedback controllers [23], [26]. For the HDEA, the distinct feature is the sustained heating-dominated behavior, which is emphasized in this work. Detailed validation of disturbance decomposition is presented in the supplementary material.

Taking its unique nonlinear electromechanical transition effect into consideration, the dynamic model of the HDEA can be further simplified as a cascading system comprising an electromechanical transduction module and a linear system $G(z)$ along with the equivalent disturbances (Fig. 4a). To obtain the specific dynamic model, $G(z)$ is identified from the chirp results:

$$G(z) = z^{-7} \times 10^{3} \times \frac{2.362z^5 - 8.916z^4 + 10.787z^3 - 6.397z^2 + 1.445z}{z^5 - 3.615z^4 + 4.671z^3 - 2.283z^2 + 0.017z + 0.211} \tag{3}$$

It can be seen that despite the temperature drift leading to displacement drift and certain model errors, the identified model still captures the frequency responses in Fig. 5. Meanwhile, the equivalent disturbance is plotted in the supplementary material (Fig. S1 and Table S1). The disturbance not only demonstrates periodic and bounded characteristics (less than 15% across the operating frequency range), but also shows a drift trend in the high-frequency range, validating the aforementioned assumption. Employing the zero-phase-error-tracking approach [37], the stable approximate inverse model $G_{inv}(z)$ can be obtained as:

$$G_{inv}(z) = 10^{-3} \times \frac{z^5 - 3.615z^4 + 4.671z^3 - 2.283z^2 + 0.017z + 0.211}{2.362z^5 - 8.916z^4 + 10.787z^3 - 6.397z^2 + 1.445z} \tag{4}$$

The related delay term z^{-m} is generated through:

$$z^{-m} = G(z)\, G_{inv}(z) = z^{-7} \tag{5}$$

Considering the nonlinear electromechanical effect, the square and root modules are introduced in the scheme for a unit dimension. Then, a spectrum-selection filter $Q(z)$ is introduced. Its output is further plugged into the existing closed-loop control system, generating the transfer function between the reference trajectory $y_r(k)$ and the error $e(k)$:

$$S(z) \approx \frac{1 - z^{-m} Q(z)}{1 + G(z)\, C(z)} \tag{6}$$

where $C(z)$ refers to the original closed-loop controller. By designing the spectrum-selection filter $Q(z)$ to form a comb-like magnitude response in the above transfer function [33], the modified repetitive control (MRC) scheme tailored for HDEA is established, which can achieve high-precision tracking at the fundamental frequency and its harmonics. However, this strict notch-filter property leads to error amplification at non-harmonic frequencies, manifesting the unavoidable sensitivity

Authorized licensed use limited to: Shanghai Jiaotong University. Downloaded on November 05,2026 at 09:43:44 UTC from IEEE Xplore. Restrictions apply.
© 2026 IEEE. All rights reserved, including rights for text and data mining and training of artificial intelligence and similar technologies. Personal use is permitted, but republication/redistribution requires IEEE permission. See https://www.ieee.org/publications/rights/index.html for more information.

This article has been accepted for publication in IEEE Transactions on Automation Science and Engineering. This is the author's version which has not been fully edited and content may change prior to final publication. Citation information: DOI 10.1109/TASE.2026.3748659

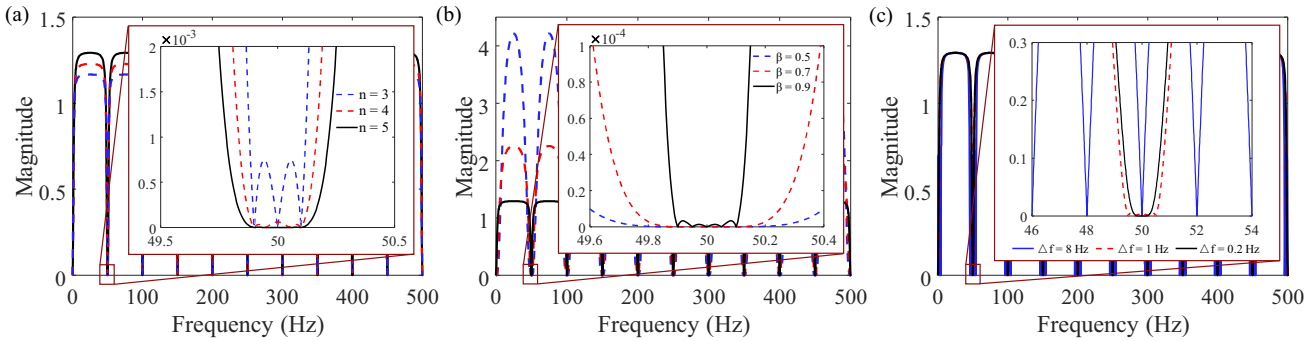


Fig. 6. The magnitude responses of the band-stop filter $V(z)$ with different (a) numbers of notch frequencies n; (b) values of β; (c) stopband bandwidth Δf.

towards reference frequency uncertainty. Hence, the above limitations lead to a large tracking error when the reference frequency deviates from its adjacent harmonics, limiting its application within a wide bandwidth.

To address these limitations, the key element is to involve a stop band in the closed-loop response [38]. In equation (6), the amplitude-frequency characteristic is determined by the term $1 - z^{-m}Q(z)$, indicating an indirect scalability with the $Q(z)$ design. Here, as shown in Fig. 4(b), the structure of the spectrum-selection filter $Q(z)$ is redesigned as:

$$\begin{aligned} Q(z) &= z^{m+r}(1 - V(z))\frac{q(z, z^{-1})}{z^r} \\ &= z^{m+r}(1 - V(z))\frac{(az^{-1} + b + az)^i}{z^r} \end{aligned} \tag{7}$$

Here $q(z, z^{-1})$ is a zero-phase low-pass filter for closed-loop system stability, which eliminates the high-frequency noise in the system. r is the delay term for its implementation. With this controller design (Fig. 4b), the transfer function can be rewritten as:

$$\begin{aligned} S(z) &\approx \frac{1 - q(z, z^{-1}) + V(z)q(z, z^{-1})}{1 + G(z)C(z)} \\ &\approx \frac{V(z)}{1 + G(z)C(z)} \end{aligned} \tag{8}$$

Hence, the closed-loop response can be regulated directly by the term $V(z)$, which will be investigated in the next subsection.

B. Band-stop filter design

To obtain a proper closed-loop response, a band-stop filter is further designed based on the above scheme [38]. To expand the effective frequency range of the MRC method, the initial filter $V(z)$ is designed with an offset as:

$$\tilde{V}(z) = \frac{1 - e^{i2\pi\frac{d_f}{f_0}}z^{-N}}{1 - e^{i2\pi\frac{d_f}{f_0}}\beta z^{-N}} \tag{9}$$

where f_0 is the fundamental frequency, d_f refers to the related offset of notch frequency. N is the sample quantity within one fundamental period. β is the crucial parameter for magnitude response adjustment. Its basic magnitude response is plotted with the dashed line in Fig. 4(c). Due to its conjugated feature, cascading multiple $V(z)$ with symmetric d_f can form a stop band around the isolated fundamental frequency f_0, as illustrated by the black line in Fig. 4(c). Hence, by distributing the notch frequencies uniformly on the stop band, the developed band-stop filter $V(z)$ can be written as:

i) when n is an even number:

$$V(z) = \frac{\prod_{j=1}^{\frac{n}{2}}(1 - \cos(2\pi j\frac{\Delta f}{nf_0})z^{-N} + z^{-2N})}{\prod_{j=1}^{\frac{n}{2}}(1 - \cos(2\pi j\frac{\Delta f}{nf_0})z^{-N} + \beta^2 z^{-2N})} \tag{10}$$

ii) when n is an odd number:

$$\begin{aligned} V(z) = &\frac{1 - z^{-N}}{1 - \beta z^{-N}} \times \\ &\frac{\prod_{j=1}^{\frac{n-1}{2}}(1 - 2\cos(2\pi j\frac{\Delta f}{nf_0})z^{-N} + z^{-2N})}{\prod_{j=1}^{\frac{n-1}{2}}(1 - 2\cos(2\pi j\frac{\Delta f}{nf_0})z^{-N} + \beta^2 z^{-2N})} \end{aligned} \tag{11}$$

where Δf represents the stopband bandwidth, and n is the number of notch points in the stopband. Based on this configuration, the robustness towards frequency uncertainty is improved, forming a modified robust repetitive control (MRRC) scheme for HDEA. To evaluate the parameter influence on the closed-loop response performance, the amplitude-frequency characteristic with different β, n, and Δf is analyzed. Key observations include:

i) As illustrated in Fig. 6(a), increasing n, corresponding to more cascaded filters in the narrow band, enhances the band-stop performance of the controller, whereas its comb-like response leads to an accompanying gain amplification at non-harmonic frequencies. To enhance the band-stop performance, n is chosen as 5 (solid line in Fig. 6a).

ii) Fig. 6(b) demonstrates that increasing β provides limited amplification at unrelated frequencies, thus improving the tracking accuracy. The frequency sensitivity around the stop band is simultaneously restricted (solid line). For high tracking precision, β is chosen as 0.96 in the following experiments.

iii) With the increase of the stopband bandwidth Δf, the band-stop performance at the unnotched frequency gradually damps. Hence, band-stop performance gradually transfers to the spectrum selection on isolated notch frequencies, indicating a rational selection of Δf in the practical implementation

Authorized licensed use limited to: Shanghai Jiaotong University. Downloaded on November 05,2026 at 09:43:44 UTC from IEEE Xplore. Restrictions apply.
© 2026 IEEE. All rights reserved, including rights for text and data mining and training of artificial intelligence and similar technologies. Personal use is permitted, but republication/redistribution requires IEEE permission. See https://www.ieee.org/publications/rights/index.html for more information.

This article has been accepted for publication in IEEE Transactions on Automation Science and Engineering. This is the author's version which has not been fully edited and content may change prior to final publication. Citation information: DOI 10.1109/TASE.2026.3748659

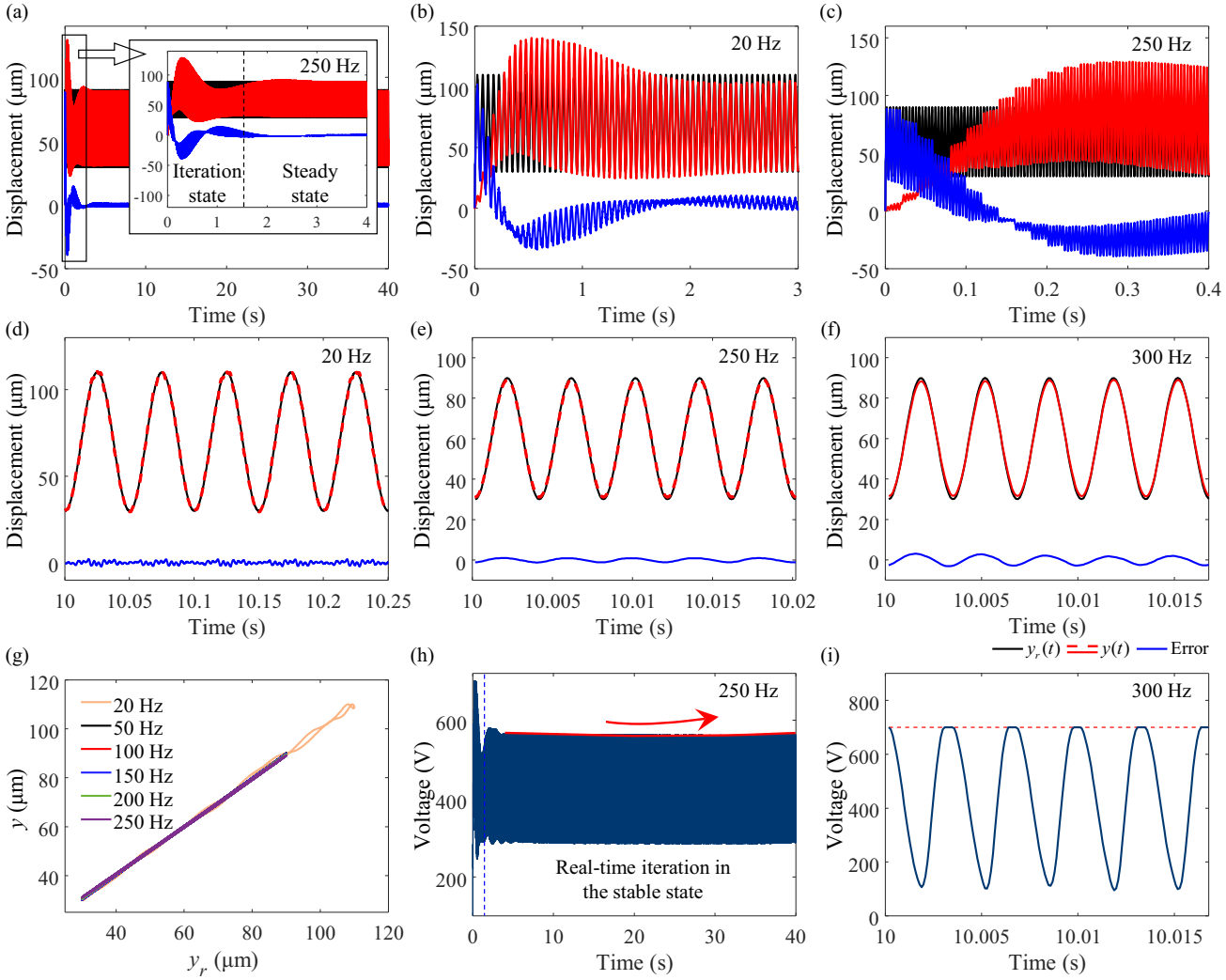


Fig. 7. The experimental results of tracking different sinusoidal trajectories. (a) The whole tracking process at 250 Hz. Iteration process at (b) 20 Hz and (c) 250 Hz. Stable tracking at (d) 20 Hz, (e) 250 Hz, and (f) 300 Hz. (g) The linearized relationship between the reference and actual displacement. (h) Control voltage at 250 Hz. (i) The saturated control voltage at 300 Hz.

(Fig. 6c). Considering the work frequency range, the fundamental frequency f_0 and the stopband bandwidth Δf in the MRRC scheme are respectively set as 50 Hz and 0.2 Hz to form a narrow stop band (black line in Fig. 6c). Further discussion about the Δf will be provided in Section V.

Due to its robustness and ease of implementation, a proportional-integral (PI) controller is employed as the baseline closed-loop controller $C(z)$. Its parameters are chosen by a trial-and-error method, set as $k_p = 1\times10^{-4}$, $k_i = 6\times10^{-4}$. Considering the high-frequency noise, the parameters in the low-pass filter are set as $a = 0.45$, $b = 0.1$, and $i = r = 3$, respectively. Further discussion on the parameter selection will be presented in the Discussion Section. Also, the supplementary material provides the closed-loop stability validation (Page. 4 in the supplementary material). Based on the designed MRRC, its control performance is then characterized.

IV. Experimental Validation

To verify the efficacy of the established MRRC method, the sinusoidal references are first employed as:

$$y_r(t) = \frac{A}{2}\sin(2\pi f t - \frac{\pi}{2}) + \frac{A}{2} + B(\mu m) \qquad (12)$$

where A, B, and f are referred to as the amplitude, bias, and frequency of the sinusoidal trajectory, respectively. Fig. 7(a) shows one example of the experimental results at an operating frequency of 250 Hz. In the initial time, the MRRC scheme takes a finite time to converge and then achieves stable tracking. The reason is that, as a learning control strategy, the MRRC scheme needs a finite iteration time. The duration is set to 40 seconds to fully demonstrate its tracking capacity in the high-frequency actuation. Without loss of generality, taking the maximum error of 10% as the classification criterion, the whole experimental process can be divided into iteration and stable states (Fig. 7a). Fig. 7(b) and (c) provide specific iteration processes in different tracking experiments. It can be seen that the closed-loop system converges in a short time

Authorized licensed use limited to: Shanghai Jiaotong University. Downloaded on November 05,2026 at 09:43:44 UTC from IEEE Xplore. Restrictions apply.
© 2026 IEEE. All rights reserved, including rights for text and data mining and training of artificial intelligence and similar technologies. Personal use is permitted, but republication/redistribution requires IEEE permission. See https://www.ieee.org/publications/rights/index.html for more information.

This article has been accepted for publication in IEEE Transactions on Automation Science and Engineering. This is the author's version which has not been fully edited and content may change prior to final publication. Citation information: DOI 10.1109/TASE.2026.3748659

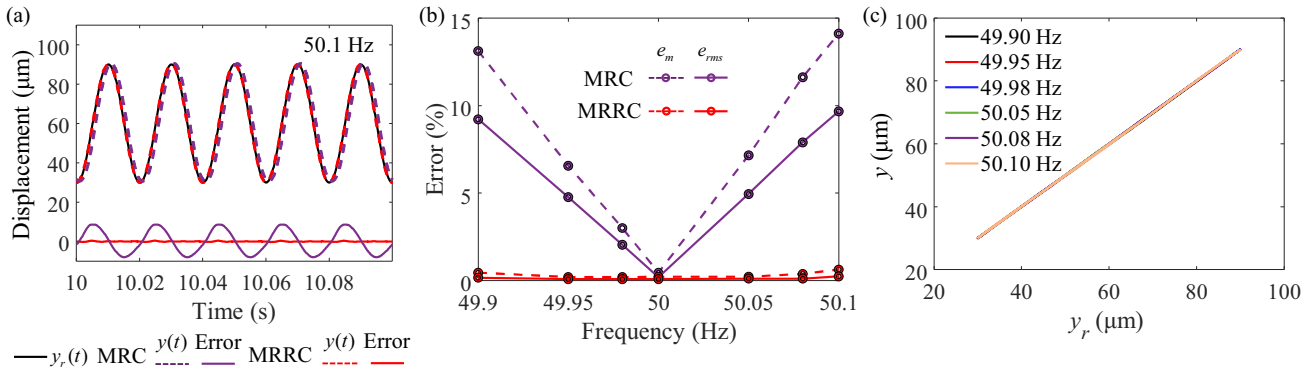


Fig. 8. The experimental results with the MRRC scheme within the stop band. (a) Tracking results comparison within the expanded stop band. (b) Detailed tracking error comparison. (c) The linearized relationship between the reference displacement and output displacement within the stop band.

with a certain overshoot. For efficacy demonstration, in the following part, the experimental results are extracted from the stable state.

The experimental results in Fig. 7(d) and (e) demonstrate that the MRRC achieves high-precision tracking at the fundamental frequency and its harmonics. Considering the larger reachable workspace in the low-frequency range, setting the fundamental frequency f_0 to 20 Hz allows tracking a larger reference (Fig. 7d). Hence, the coupled viscoelasticity, mechanical vibration, and temperature drift of the HDEA are compensated by the MRRC scheme within a wide frequency range (Fig. 7g). The temperature change in the HDEA mainly comes from the continuous heating in the actuation process, manifesting a sustained slow drift in the high-frequency displacement. As a real-time learning control strategy, the MRRC scheme introduces a real-time iteration in the control voltage (Fig. 7h), thus mitigating the error introduced by the heating. As shown in Fig. 7(f), larger tracking errors can be observed at 300 Hz, which is due to the control voltage saturation (Fig. 7i). Further discussion about the voltage saturation and corresponding tracking performance deterioration is presented in the Discussion Section.

Remark: The application of the MRRC in the lower frequency range corresponds to a lower fundamental frequency, thus, more delay items in the control module. Due to our hardware limitation, the lower frequency bound in this work is set as 20 Hz.

To further provide a quantitative view, the absolute error e_{ab}, maximum error e_m, and root-mean-square error e_{rms} are respectively defined as:

$$e_{ab} = |y_r - y| \tag{13}$$

$$e_m = \frac{|y_r - y|}{\max(y_r) - \min(y_r)} \times 100\% \tag{14}$$

$$e_{rms} = \frac{\sqrt{\frac{1}{N}\sum_{i=1}^{N}(y_r - y)^2}}{\max(y_r) - \min(y_r)} \times 100\% \tag{15}$$

where y_r and y are the reference and actual displacement, respectively. N is the sample quantity in one period. The aforementioned errors are systematically listed in Table I. The micron-order tracking errors underscore the capacity of the proposed MRRC scheme in the HDEA control realm.

Meanwhile, repeated tracking experiments are conducted on a newly built experimental platform. To validate its effectiveness in mitigating such intricate nonlinearity, comparison experiments with different controllers (PID and nonlinear sliding-mode control [28]) are conducted. Detailed tracking results are presented in Fig. S2 and Table S2 (supplementary material). The controller is also employed under different environmental conditions, as shown in Fig. S3. These results not only demonstrate that the MRRC effectively improves the tracking speed compared with these controllers, but also prove the credibility of the control scheme.

TABLE I
TRACKING ERRORS UNDER DIFFERENT FREQUENCIES

Controller	Without		MRRC			
f (Hz)	e_m (%)	e_{rms} (%)	f_0 (Hz)	e_{ab} (μm)	e_m (%)	e_{rms} (%)
20	41.68	19.70	20	2.15	2.69	1.06
50	50.98	25.72		0.13	0.22	0.09
100	69.60	34.65		0.17	0.28	0.16
150	58.37	36.54	50	0.29	0.48	0.29
200	67.26	46.98		0.63	1.04	0.70
250	95.18	67.21		1.11	1.84	1.26

To demonstrate its reduced frequency sensitivity, the MRRC scheme is employed in the given stopband, as shown in Fig. 8. Also, an MRC scheme (without the integrated band-stop filter) is established for comparison. It can be seen that a slight frequency deviation in the reference inevitably leads to a large tracking error in the MRC scheme due to its high frequency sensitivity. In comparison, the MRRC scheme demonstrates its robustness towards frequency uncertainty. Specifically, the tracking performance on the unnotched frequency proves a continuous stopband around the original effective frequency. For comprehensive comparison, detailed tracking error, overshoot (compared to the stable tracking state, noted as δ), and convergence speed (the number of iterations to reach the steady state, noted as N_{conv}) are presented in Table II. In the stopband, though with a larger overshoot, the MRRC can

Authorized licensed use limited to: Shanghai Jiaotong University. Downloaded on November 05,2026 at 09:43:44 UTC from IEEE Xplore. Restrictions apply.
© 2026 IEEE. All rights reserved, including rights for text and data mining and training of artificial intelligence and similar technologies. Personal use is permitted, but republication/redistribution requires IEEE permission. See https://www.ieee.org/publications/rights/index.html for more information.

This article has been accepted for publication in IEEE Transactions on Automation Science and Engineering. This is the author's version which has not been fully edited and content may change prior to final publication. Citation information: DOI 10.1109/TASE.2026.3748659

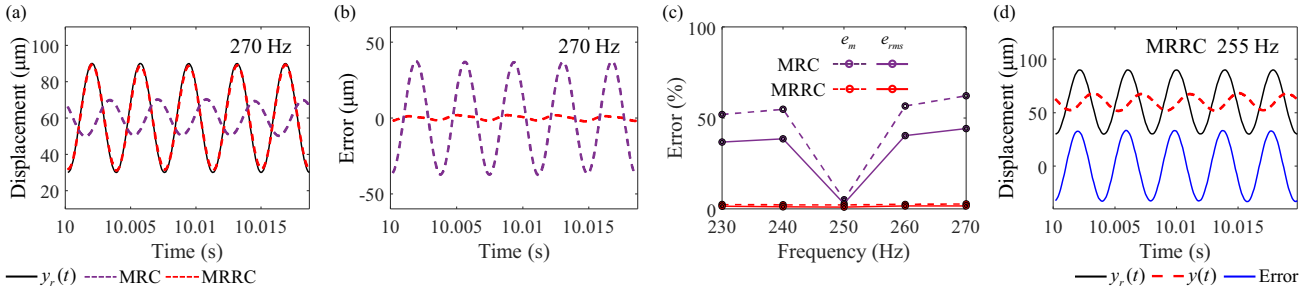


Fig. 9. The experimental results with different stopband bandwidths in the MRRC. (a) - (b) Tracking results comparison at the notch frequency (270 Hz). (c) Detailed tracking error comparison. (d) Tracking results of the MRRC scheme at the unnotched frequency (255 Hz).

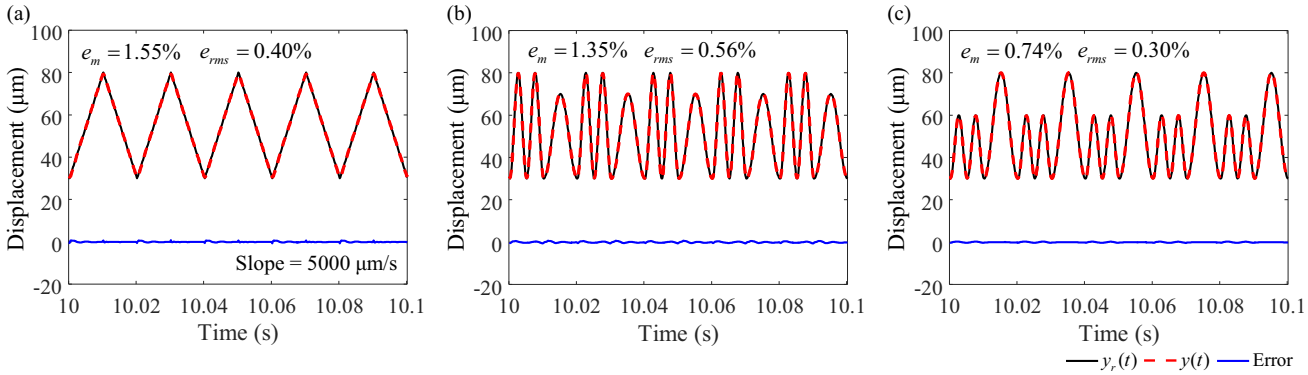


Fig. 10. Tracking results of more trajectories. (a) Triangular trajectory. (b) - (c) Complex periodic trajectories.

TABLE II
TRACKING ERRORS IN THE ATTENUATION BAND

Controller	Without		MRC				MRRC				
f (Hz)	e_m (%)	e_{rms} (%)	e_m (%)	e_{rms} (%)	δ (%)	N_{conv}	e_{ab} (μm)	e_m (%)	e_{rms} (%)	δ (%)	N_{conv}
49.9	50.95	25.52	13.12	9.22	8.49	114	0.27	0.46	0.17	36.58	71
49.95	50.26	25.28	6.57	4.77	7.33	142	0.13	0.21	0.09	36.19	71
49.98	50.50	25.11	3.01	2.05	7.24	169	0.13	0.21	0.09	37.42	72
50	50.98	25.72	0.46	0.20	7.17	73	0.13	0.22	0.09	35.69	71
50.05	49.68	25.11	7.16	4.95	6.87	132	0.13	0.22	0.12	35.08	71
50.08	50.08	24.83	11.62	7.90	6.87	111	0.23	0.39	0.12	36.39	71
50.1	50.51	25.10	14.11	9.67	6.86	105	0.39	0.64	0.25	36.67	71

quickly converge to achieve high-precision tracking compared with the MRC scheme.

V. DISCUSSION

The aforementioned parameter setting in $V(z)$ achieves a continuous but narrow band-stop effect. To reduce the frequency sensitivity in a wider frequency range, the stopband width is increased, which is then translated to isolated but distant effective notch frequencies (blue line in Fig. 6c). Here, to fully demonstrate the tracking performance of the MRRC scheme in the high-frequency range, the fundamental frequency f_0 and stopband width Δf are set to 250 and 40 Hz, respectively.

The corresponding results are shown in Fig. 9 and Table III. Compared with the MRC strategy, the MRRC scheme achieves an error decrease of around 100% on the expanded notch frequencies, facilitating its practical application in the HDEA realm. However, a tremendous tracking error is found at the unnotched frequency (Fig. 9d). The main reason comes from the error amplification effect in these frequency ranges, indicating a trade-off based on practical applications. Table III also presents the slightly larger overshoot in the MRRC scheme. The distinctly different iteration time in the MRC scheme can be attributed to the gain amplification effect at nonharmonic frequencies. The experimental results demonstrate that the sinusoidal trajectory of 270 Hz can be precisely tracked (Fig. 9a), while larger errors can be observed at 300 Hz (Fig. 7f). This phenomenon can be attributed to the dynamic response and voltage limitation of the HDEA. The available displacement range rapidly decreases with increasing frequency exceeding the natural frequency, which indicates a high input voltage to achieve a certain workspace. Whereas, to avoid electrical breakdown and performance attenuation, the input voltage is set below 700 V. When tracking a high-

Authorized licensed use limited to: Shanghai Jiaotong University. Downloaded on November 05,2026 at 09:43:44 UTC from IEEE Xplore. Restrictions apply.
© 2026 IEEE. All rights reserved, including rights for text and data mining and training of artificial intelligence and similar technologies. Personal use is permitted, but republication/redistribution requires IEEE permission. See https://www.ieee.org/publications/rights/index.html for more information.

This article has been accepted for publication in IEEE Transactions on Automation Science and Engineering. This is the author's version which has not been fully edited and content may change prior to final publication. Citation information: DOI 10.1109/TASE.2026.3748659

TABLE III
TRACKING ERRORS WITH DIFFERENT STOPBAND BANDWIDTH IN THE MRRC

Controller	Without		MRC				MRRC				
f (Hz)	e_m (%)	e_{rms} (%)	e_m (%)	e_{rms} (%)	δ (%)	N_{conv}	e_{ab} (μm)	e_m (%)	e_{rms} (%)	δ (%)	N_{conv}
230	82.96	57.89	51.92	36.78	9.60	30	1.45	2.41	1.48	12.33	184
240	89.69	62.78	54.75	38.55	10.56	30	1.35	2.25	1.15	10.14	142
250	95.18	67.21	5.12	2.88	5.72	152	1.86	3.09	1.44	9.69	138
260	97.91	69.16	56.55	40.26	9.96	31	1.52	2.53	1.58	9.58	143
270	99.71	71.08	62.18	44.23	7.99	33	1.65	2.75	1.71	9.55	151

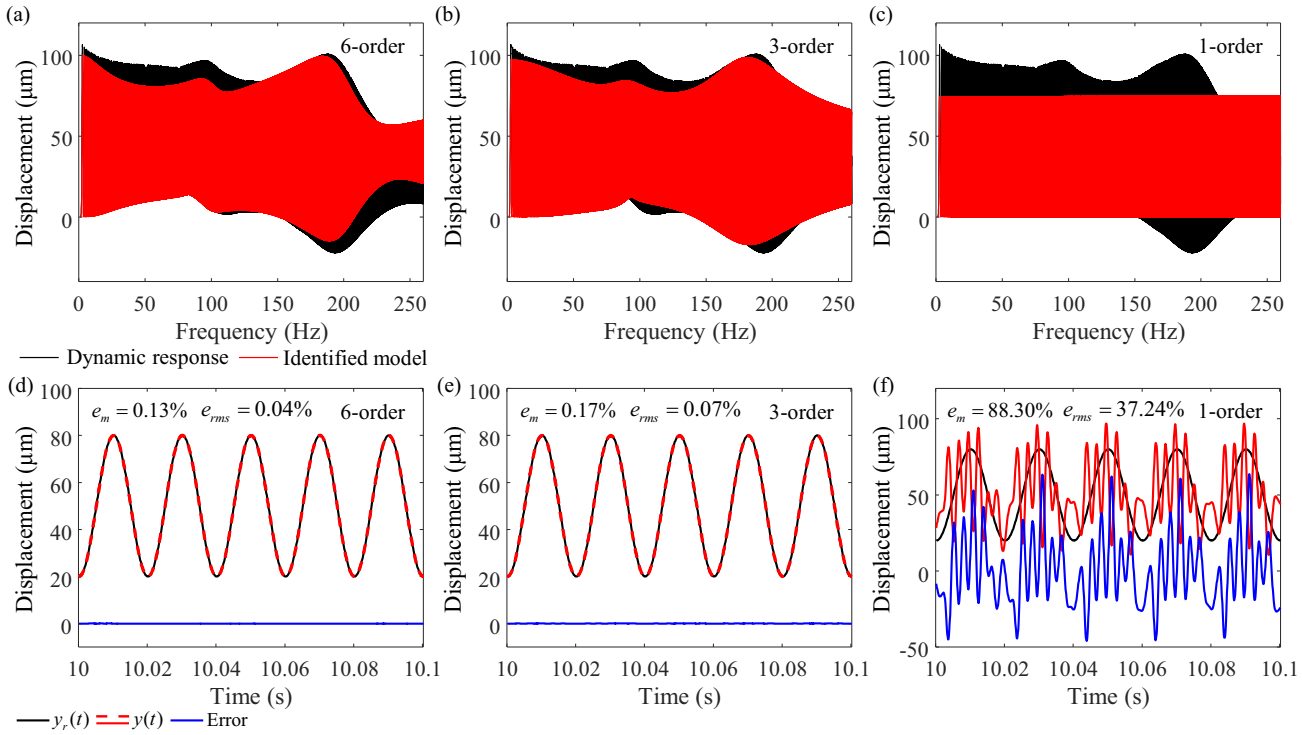


Fig. 11. The comparison of the experimental data and identified model with different orders. (a) 6-order; (b) 3-order; (c) 1-order. The corresponding tracking results with different model orders: (d) 6-order; (e) 3-order; (f) 1-order.

frequency reference, the control voltage amplitude increases and triggers the preset saturation (Fig. 7i and Fig. S4). Thus, based on the specific experimental setup, the maximum working frequency is characterized as 270 Hz in this work.

Through different filter parameter settings, high-precision tracking is achieved under different frequencies. Detailed results are shown in Fig. S5 and Table S3, further validating the effectiveness of the controller. Then the MRRC scheme is employed to track complex periodic references. The experimental results in Fig. 10 validate the MRRC scheme's capacity to track diverse trajectories.

To investigate how controller parameters affect control performance, tracking experiments are first carried out based on $G(z)$ with different orders. As shown in Fig. 11, larger model error in the low-order $G(z)$ leads to worse tracking performance. This indicates the proper choice of linear system order for better tracking performance. Meanwhile, reducing the filter parameter β, reducing the low-pass filter parameter will weaken the suppression effect on high-frequency noise. Hence, high-frequency oscillations can be observed in the control voltage, thus leading to larger tracking errors (Fig. 12).

Next, the physical limitation in this work is discussed. The aforementioned results in Fig. 7 indicate that the high-frequency tracking is limited by the voltage saturation. Improving the manufacturing technique can improve the quality of the dielectric elastomer membrane, enabling the breakdown voltage improvement. Another potential limitation comes from the sustained temperature rise at high frequencies, which manifests as displacement drift over time. Due to the online learning nature of the MRRC strategy, the control voltage evolves throughout the experiments (Fig. 7h and Fig. S6), potentially triggering voltage saturation in sustained tracking. This may deteriorate tracking performance in long-duration high-speed tracking. Since the thermal-induced behavior mainly comes from the damping effect of the HDEA, new compliant electrode materials with reduced resistance will help to overcome this limitation.

Authorized licensed use limited to: Shanghai Jiaotong University. Downloaded on November 05,2026 at 09:43:44 UTC from IEEE Xplore. Restrictions apply.
© 2026 IEEE. All rights reserved, including rights for text and data mining and training of artificial intelligence and similar technologies. Personal use is permitted, but republication/redistribution requires IEEE permission. See https://www.ieee.org/publications/rights/index.html for more information.

This article has been accepted for publication in IEEE Transactions on Automation Science and Engineering. This is the author's version which has not been fully edited and content may change prior to final publication. Citation information: DOI 10.1109/TASE.2026.3748659

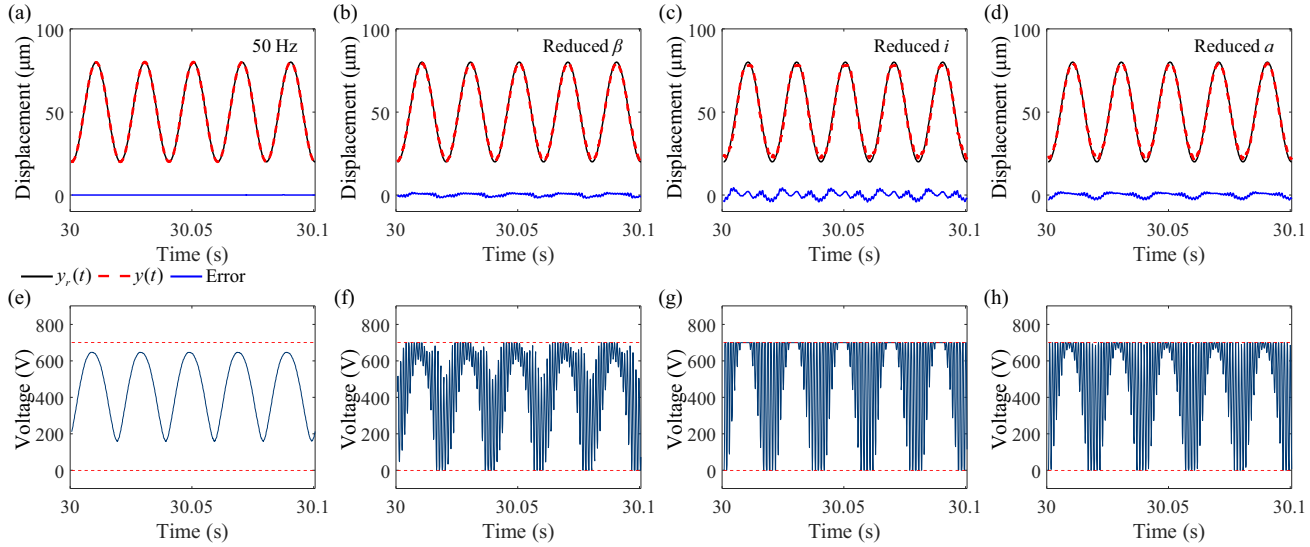


Fig. 12. (a) - (d) Tracking results with different controller parameters. (e) - (h) The corresponding control voltages.

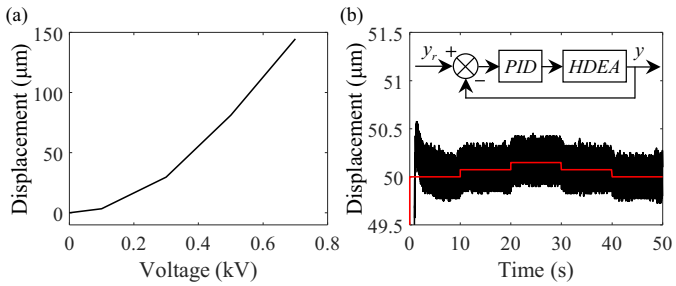


Fig. 13. Performance characterization. (a) Stroke. (b) Resolution.

It should be mentioned that the MRRC scheme uses the tracking error for periodic iteration. Its basic principle intrinsically requires the reference trajectories to be periodic, making it inapplicable to non-periodic references. Furthermore, its online iteration demands multiple operating cycles, introducing compensation delay in transient trajectory tracking. The errors arising from transient references will be retained by the controller, producing excessive control actions and additional disturbances in subsequent operating cycles. Hence, the MRRC scheme exhibits inherent limitations for tracking non-periodic and transient reference trajectories.

Further, a step voltage is employed to reveal the stroke of the stacked HDEA. The stroke is defined as the displacement after 2 s with the step excitation voltage. As shown in Fig. 13(a), the stroke demonstrates a positive correlation with the voltage amplitude. The maximum stroke reaches 144 μm. To evaluate its displacement resolution, a 75 nm step command is utilized in a closed-loop PID control system. The measured displacement is illustrated in Fig. 13(b), demonstrating a ten-nanometer-level resolution. These results indicate the potential application of HDEA in the micro-manipulation systems [39].

Overall, with reduced frequency sensitivity, the MRRC achieves high-precision control of the HDEA up to 270 Hz with micron-order accuracy, mitigating the coupled rate-dependent viscoelasticity, mechanical vibration, and temperature drift within a wide frequency range. Additional tests are conducted to examine the proposed MRRC scheme with an enlarged stop-band width. Tracking experiments of various trajectories verify its effectiveness, and critical factors influencing tracking performance are uncovered.

VI. Conclusion

This work proposes a modified robust repetitive control (MRRC) scheme for high-speed dielectric elastomer actuators (HDEAs) to achieve high-precision tracking. A customized experimental platform is first established based on a stacked DEA. Based on the experimental setup, the nonlinear dynamic responses are investigated. To achieve high-precision control, the repetitive control strategy is introduced in the HDEA realm based on dynamic model simplification. The MRRC scheme is then established by scheme design and filter implementation, thus forming a stop band in the closed-loop frequency response. The experimental validation details its capacity to mitigate the rate-dependent viscoelasticity, mechanical vibration, temperature drift, and their couplings across a wide frequency spectrum. Further exploration provides an in-depth perspective of the MRRC strategy, including different stopband bandwidths, diverse references, and key factors influencing the tracking performance. Future efforts can focus on multi-degree micro-manipulation systems actuated by HDEAs.

References

[1] G. Li, X. Chen, F. Zhou *et al.*, "Self-powered soft robot in the mariana trench," *Nature*, vol. 591, no. 7848, pp. 66–71, 2021.
[2] W. Yu, W. Zheng, S. Hua *et al.*, "A prestretch-free dielectric elastomer with record-high energy and power density via synergistic polarization enhancement and strain stiffening," *Advanced Functional Materials*, vol. 35, no. 35, p. 2425099, 2025.
[3] G. Gu, J. Zou, R. Zhao *et al.*, "Soft wall-climbing robots," *Science Robotics*, vol. 3, no. 25, p. eaat2874, 2018.
[4] X. Wang, S. Li, J.-C. Chang *et al.*, "Multimodal locomotion ultra-thin soft robots for exploration of narrow spaces," *Nature Communications*, vol. 15, no. 1, p. 6296, 2024.
[5] E. Hajiesmaili and D. R. Clarke, "Dielectric elastomer actuators," *Journal of Applied Physics*, vol. 129, no. 15, p. 151102, 2021.

Authorized licensed use limited to: Shanghai Jiaotong University. Downloaded on November 05,2026 at 09:43:44 UTC from IEEE Xplore. Restrictions apply.
© 2026 IEEE. All rights reserved, including rights for text and data mining and training of artificial intelligence and similar technologies. Personal use is permitted, but republication/redistribution requires IEEE permission. See https://www.ieee.org/publications/rights/index.html for more information.

This article has been accepted for publication in IEEE Transactions on Automation Science and Engineering. This is the author's version which has not been fully edited and content may change prior to final publication. Citation information: DOI 10.1109/TASE.2026.3748659

[6] S. Xu, Y. Chen, N.-s. P. Hyun *et al.*, "A dynamic electrically driven soft valve for control of soft hydraulic actuators," *Proceedings of the National Academy of Sciences*, vol. 118, no. 34, p. e2103198118, 2021.
[7] M. Duduta, E. Hajiesmaili, H. Zhao *et al.*, "Realizing the potential of dielectric elastomer artificial muscles," *Proceedings of the National Academy of Sciences*, vol. 116, no. 7, pp. 2476–2481, 2019.
[8] L. Wang, J. Zhuo, J. Peng *et al.*, "A stretchable soft pump driven by a heterogeneous dielectric elastomer actuator," *Advanced Functional Materials*, vol. 34, no. 52, p. 2411160, 2024.
[9] H. Zhao, A. M. Hussain, M. Duduta *et al.*, "Compact dielectric elastomer linear actuators," *Advanced Functional Materials*, vol. 28, no. 42, p. 1804328, 2018.
[10] J.-H. Youn, S.-Y. Jang, I. Hwang *et al.*, "Skin-attached haptic patch for versatile and augmented tactile interaction," *Science Advances*, vol. 11, no. 12, p. eadt4839, 2025.
[11] C. Tang, B. Du, S. Jiang *et al.*, "A pipeline inspection robot for navigating tubular environments in the sub-centimeter scale," *Science Robotics*, vol. 7, no. 66, p. eabm8597, 2022.
[12] Y. Chen, H. Zhao, J. Mao *et al.*, "Controlled flight of a microrobot powered by soft artificial muscles," *Nature*, vol. 575, no. 7782, pp. 324–329, 2019.
[13] Y. Zhang, Y. Wang, J. Wu *et al.*, "Inverse compensation-based global fast terminal integral sliding mode control with lumped uncertainty fuzzy estimation for dielectric electro-active polymer actuator," *IEEE Transactions on Fuzzy Systems*, vol. 32, no. 10, pp. 5791–5801, 2024.
[14] C. Cao, C. Wu, X. Li *et al.*, "A quad-unit dielectric elastomer actuator for programmable two-dimensional trajectories," *Advanced Intelligent Systems*, vol. 6, no. 5, p. 2300865, 2024.
[15] H. Zhao, A. M. Hussain, A. Israr *et al.*, "A wearable soft haptic communicator based on dielectric elastomer actuators," *Soft Robotics*, vol. 7, no. 4, pp. 451–461, 2020.
[16] T. Hoffstadt and J. Maas, "Adaptive sliding-mode position control for dielectric elastomer actuators," *IEEE/ASME Transactions on Mechatronics*, vol. 22, no. 5, pp. 2241–2251, 2017.
[17] T. Lu, C. Ma, and T. Wang, "Mechanics of dielectric elastomer structures: A review," *Extreme Mechanics Letters*, vol. 38, p. 100752, 2020.
[18] G.-h. Miao, C. Yuan, X.-y. Chu *et al.*, "Study on the performance optimization of circular dielectric elastomer membrane actuator by charge compensation methods," *Acta Mechanica*, vol. 236, pp. 3629–3650, 2025.
[19] X. Lu, Y. Lin, and T. Hu, "Physic-based and control-oriented modeling based robust control for soft dielectric elastomer actuator," *Smart Materials and Structures*, vol. 29, no. 3, p. 035026, 2020.
[20] G. Rizzello, D. Naso, A. York *et al.*, "Modeling, identification, and control of a dielectric electro-active polymer positioning system," *IEEE Transactions on Control Systems Technology*, vol. 23, no. 2, pp. 632–643, 2015.
[21] Y. Wang, X. Zhang, Z. Li *et al.*, "Adaptive implicit inverse control for a class of butterfly-like hysteretic nonlinear systems and its application to dielectric elastomer actuators," *IEEE Transactions on Industrial Electronics*, vol. 70, no. 1, pp. 731–740, 2023.
[22] Z. Li, Z. Li, H. Xu *et al.*, "Development of a butterfly fractional-order backlash-like hysteresis model for dielectric elastomer actuators," *IEEE Transactions on Industrial Electronics*, vol. 70, no. 2, pp. 1794–1801, 2023.
[23] Y. Wang, P. Huang, J. Wu *et al.*, "Modelling and compound control of intelligently dielectric elastomer actuator," *Control Engineering Practice*, vol. 126, p. 105261, 2022.
[24] X. Zhang, Y. Liu, X. Chen *et al.*, "Adaptive pseudoinverse control for constrained hysteretic nonlinear systems and its application on dielectric elastomer actuator," *IEEE/ASME Transactions on Mechatronics*, vol. 28, no. 4, pp. 2142–2154, 2023.
[25] P. Huang, J. Wu, C.-Y. Su *et al.*, "Tracking control of soft dielectric elastomer actuator based on nonlinear PID controller," *International Journal of Control*, vol. 97, no. 1, pp. 130–140, 2024.
[26] J. Zou, S. O. Kassim, J. Ren *et al.*, "A generalized motion control framework of dielectric elastomer actuators: Dynamic modeling, sliding-mode control and experimental evaluation," *IEEE Transactions on Robotics*, vol. 40, pp. 919–935, 2024.
[27] J. Lv, H. Hong, Z. Gan *et al.*, "Nonlinear dynamic modeling and control of 2-DOF tunable prism driven by dielectric elastomer," *IEEE Transactions on Automation Science and Engineering*, vol. 23, pp. 2511–2525, 2026.
[28] S. O. Kassim, P. Yan, X. Chen *et al.*, "A triple power reaching law-enhanced exponential power sliding mode framework for precise high-speed tracking in dielectric elastomer actuators," *Control Engineering Practice*, vol. 171, p. 106850, 2026.
[29] L. Li, J. Li, L. Qin *et al.*, "Deep reinforcement learning in soft viscoelastic actuator of dielectric elastomer," *IEEE Robotics and Automation Letters*, vol. 4, no. 2, pp. 2094–2100, 2019.
[30] Y. Zhang, J. Wu, P. Huang *et al.*, "Inverse dynamics modelling and tracking control of conical dielectric elastomer actuator based on GRU neural network," *Engineering Applications of Artificial Intelligence*, vol. 118, p. 105668, 2023.
[31] P. Huang, J. Wu, Q. Meng *et al.*, "Self-sensing motion control of dielectric elastomer actuator based on NARX neural network and iterative learning control architecture," *IEEE/ASME Transactions on Mechatronics*, vol. 29, no. 2, pp. 1374–1384, 2024.
[32] S. Hara, Y. Yamamoto, T. Omata *et al.*, "Repetitive control system: a new type servo system for periodic exogenous signals," *IEEE Transactions on Automatic Control*, vol. 33, no. 7, pp. 659–668, 1988.
[33] P. Yan, J. Feng, S. S. Aphale *et al.*, "Mitigating the coupled effects of rate-dependent viscoelasticity and mechanical resonance in dielectric elastomer actuators via modified repetitive control," *IEEE/ASME Transactions on Mechatronics*, 2024.
[34] X. Shi, J. Zou, P. Yan *et al.*, "Semiseparated biphasic bicontinuous dielectric elastomer for high-performance artificial muscle," *Science*, vol. 390, no. 6777, pp. 1044–1049, 2025.
[35] P. Yan, G. Gu, and J. Zou, "Design, modeling and control of a dielectric elastomer actuated micro-positioning stage," in *Intelligent Robotics and Applications*, H. Yang, H. Liu, J. Zou *et al.*, Eds., vol. 14270. Springer Nature Singapore, Conference Proceedings, pp. 174–185.
[36] X. Chen and M. Tomizuka, "New repetitive control with improved steady-state performance and accelerated transient," *IEEE Transactions on Control Systems Technology*, vol. 22, no. 2, pp. 664–675, 2014.
[37] M. Tomizuka, "Zero phase error tracking algorithm for digital control," *Journal of Dynamic Systems, Measurement, and Control*, vol. 109, no. 1, pp. 65–68, 1987.
[38] W. W. Huang, C. Hu, and L. M. Zhu, "Robust repetitive control of nanopositioning stages using the spectrum-selection filter with narrow passbands," *IEEE/ASME Transactions on Mechatronics*, vol. 27, no. 5, pp. 4211–4216, 2022.
[39] C. Chen, Q. Hao, J. Cao *et al.*, "Two-dimensional varifocal scanning imaging based on alvarez and decentred lenses actuated by dielectric elastomer," *Optics & Laser Technology*, vol. 167, p. 109805, 2023.



Peinan Yan received the B.E. degree (Hons.) and the Ph.D. degree (Hons.) in mechanical engineering from Shanghai Jiao Tong University, Shanghai, China, in 2020 and 2026, respectively.

His research interests include design and control of dielectric elastomer actuators.

Authorized licensed use limited to: Shanghai Jiaotong University. Downloaded on November 05,2026 at 09:43:44 UTC from IEEE Xplore. Restrictions apply.
© 2026 IEEE. All rights reserved, including rights for text and data mining and training of artificial intelligence and similar technologies. Personal use is permitted, but republication/redistribution requires IEEE permission. See https://www.ieee.org/publications/rights/index.html for more information.

This article has been accepted for publication in IEEE Transactions on Automation Science and Engineering. This is the author's version which has not been fully edited and content may change prior to final publication. Citation information: DOI 10.1109/TASE.2026.3748659



Sumeet S. Aphale (Senior Member, IEEE; CEng) is Professor of Electrical and Electronic Systems at the University of Aberdeen, U.K., where he leads the Artificial Intelligence, Robotics, and Mechatronic Systems (ARMS) Research Group. He also serves as Academic Line Manager and Research Group Leader for Electrical and Electronic Systems. His research interests include conventional and unconventional robotics, applied control, mechatronics, nonlinear dynamics, nanopositioning, and vibration suppression. His work spans fundamental control and systems research through to experimentally validated and industry-facing applications in robotics, automation, energy, and precision engineering. He has contributed to a range of nationally, internationally, and industrially funded research programmes. He is actively involved in the international control, robotics, and mechatronics communities through conference organisation, technical and programme committees, peer review, and collaborative research. Professor Aphale has served in editorial roles with IEEE Control Systems Letters, the IEEE Control Systems Society Conference Editorial Board, Frontiers in Mechanical Engineering, the International Journal of Robotics Research, and Control Engineering Practice.



Jiang Zou received the B.E. degree in mechanical engineering from the University of Science and Technology Beijing, Beijing, China, in 2014, and the Ph.D. degree in mechanical engineering from Shanghai Jiao Tong University, Shanghai, China, in 2019.

Since 2019, he has worked with Shanghai Jiao Tong University. He is currently an Associate Professor with the School of Mechanical Engineering. His research interests include dielectric elastomer based artificial muscles, soft robots, dynamic modeling and control. He has authored or coauthored more than 50 publications, which have appeared in Science, Science Robotics, Science Advances, Nature Communications, National Science Review, IEEE Transactions on Robotics, etc.



Guoying Gu (Senior Member, IEEE) received the B.E. degree (Hons.) in electronic science and technology and the Ph.D. degree (Hons.) in mechatronic engineering from Shanghai Jiao Tong University, Shanghai, China, in 2006 and 2012, respectively.

He was a Humboldt Fellow with the University of Oldenburg, Oldenburg, Germany, and was a Visiting Scholar with the Massachusetts Institute of Technology, Cambridge, MA, USA, the National University of Singapore, Singapore, and Concordia University, Montreal, QC, Canada. He is currently a Distinguished Professor with the School of Mechanical Engineering, Shanghai Jiao Tong University. He has authored or coauthored more than 150 publications, including articles in Science, Science Robotics, Nature Biomedical Engineering, Nature Reviews Materials, Nature Materials, Nature Communications, Science Advances, Advanced Materials, Soft Robotics, Science China series, the IEEE/ASME Transactions journals, book chapters, and international conference proceedings. His research interests include soft robotics, bioinspired and wearable robots, and smart materials for sensing, actuation, and motion control.

Dr. Gu was the recipient of the National Science Fund for Distinguished Young Scholars and the XPLORER Prize. He is currently an Associate Editor for Soft Robotics, Soft Science, and IEEE Transactions on Automation Science and Engineering, and was an Associate Editor for IEEE Transactions on Robotics and IEEE Robotics and Automation Letters.

Authorized licensed use limited to: Shanghai Jiaotong University. Downloaded on November 05,2026 at 09:43:44 UTC from IEEE Xplore. Restrictions apply.
© 2026 IEEE. All rights reserved, including rights for text and data mining and training of artificial intelligence and similar technologies. Personal use is permitted, but republication/redistribution requires IEEE permission. See https://www.ieee.org/publications/rights/index.html for more information.